

THIN GLASS OPTIC AND SILICON WAFER DEFORMATION AND KINEMATIC CONSTRAINT

Craig R. Forest, Mireille Akilian, Guillaume Vincent, Alexandre Lamure and Mark L. Schattenburg
Massachusetts Institute of Technology, Cambridge, MA 02139

Measuring and assembling progressively thinner (length / thickness > 6) substrates is an increasing challenge. From disk drive substrates to flat panel displays, thin glass must be mechanically maneuvered without substantial distortion. Flatness of silicon wafers in the semiconductor industry is also becoming more important.

Grazing-incidence foil-optic x-ray telescopes (such as the segmented mirror approach considered for the NASA *Constellation-X* mission) require sub-micron accurate and repeatable assembly of thousands of foils with figure errors less than 0.5 μm over their 140x100 mm² surface areas. To provide accurate metrology, a deep-UV Shack-Hartmann surface metrology system has been created [1].

To meet these assembly and metrology challenges, we present how thin materials such as silicon and glass wafers deform and how they can be constrained to minimize these effects. Both analytical calculations and finite element analyses (FEA) are utilized to understand the effects of gravity on foil deformation while varying parameters such as foil thickness and angle of inclination. Friction forces imparted during foil manipulation and thermal expansion mismatch between the foil and the constraint device are also studied.

These theoretical analyses lead to functional requirements for the design of a foil fixture—a device for holding these thin, floppy foils with kinematic mounting and minimal deformation. This air bearing device works in conjunction with the metrology system [1] to produce accurate and repeatable surface maps of the foil optics.

1. Modeling

1.1 Gravity Sag

For any simply-supported foil optic, gravity will typically cause distortions on the order of the thickness. Supported horizontally, the foil's maximum deformation will occur at its centerline as given by

$$\delta_{\max} = \frac{\rho g \sin \theta L^4}{6.4 E t^2}. \quad (1)$$

Using this equation, the deformations for 0.4 mm-thick, 140 mm-long silicon and glass foils are respectively 54 μm and 127 μm . The 0.5 μm tolerance will not allow this manner of constraint. Orienting the foils vertically effectively reduces the gravity-induced load. For a hypothetical vertical misalignment of 2 mm at the top of a 140 mm foil, the resulting angle of inclination, or pitch, of 0.82° reduces the deformation to 0.77 and 1.81 μm , respectively.

The three-dimensional deformation is more accurately modeled by FEA. This method yields a maximum displacement of 1.87 μm , for glass with dimensions 140x100x0.4 mm³, pitch of 0.82°, and pin boundary conditions, which compares well with the previous analytical beam bending result of 1.81 μm .

1.2 Boundary Conditions

To accurately simulate actual foil distortion from gravity, we need to modify the boundary conditions. We have previously assumed pin joints along the top and bottom of the foil as in Figure 1a. To avoid overconstraint in practice, we should only contact the foil's edges at three locations as in Figure 1b. In general, this triad of ball-socket joints will allow more foil sag than the pin joint edges. An FEA simulation for glass with dimensions 140x100x0.4 mm³ and pitch of 0.82° reveals a maximum deformation of 2.14 μm as compared with the previous result of 1.87 μm .

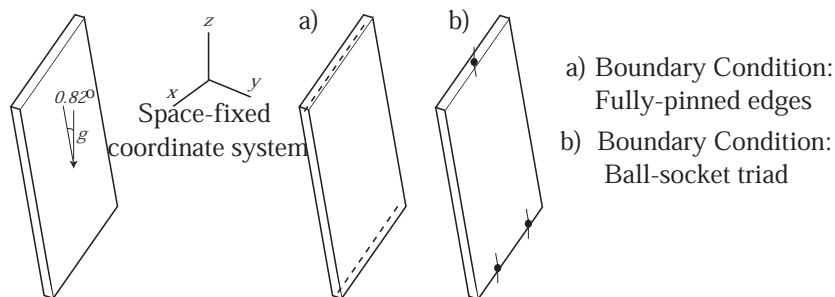


Figure 1. (a) Pin joint allows rotation about the x-axis only. (b) Ball-socket triad permits rotation about all axes.

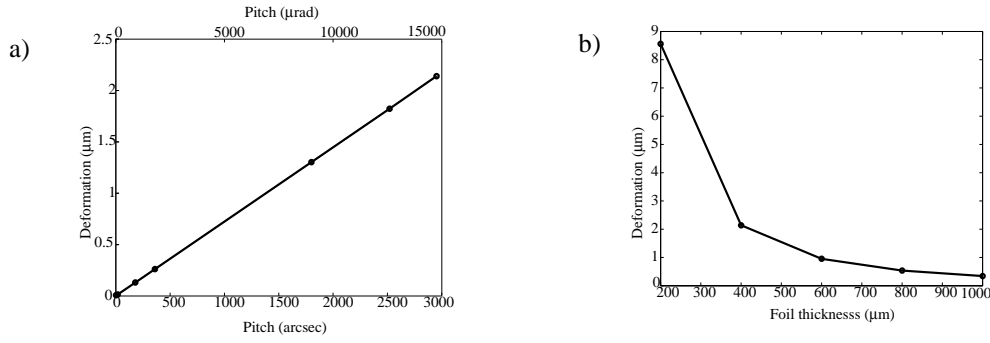


Figure 2. Maximum glass foil deformation as a function of (a) pitch angle for a thickness of 0.4 mm and (b) thickness for a pitch of 0.82°. Dimensions: 140x100 x0.4 mm³, Boundary conditions: ball-socket triad

1.3 Gravity sag as a function of pitch angle

Foil deformation as a function of pitch angle is shown in Figure 2a. These results help define the foil holder functional requirements. Specifically, if we allocate 15% of the allowable peak-valley (P-V) error (0.5 μm) to pitch angle repeatability, then this repeatability should be 100 arcsec at worst. The corresponding ~70 nm glass foil deformation should not significantly compromise assessment of the manufacturing quality.

1.4 Gravity sag as a function of foil thickness

The thickness of the foil affects how tolerant we can be of inclination errors. Equation 1 reveals that the deformation is inversely proportional to the thickness squared. Using FEA, Figure 2b shows the relationship. A 400 μm thickness was chosen for the telescope foils, balancing the needs for low mass and small deformations.

1.5 Thermal Considerations

Foil and holder expansion mismatch could inhibit accurate metrology. Linear thermal expansion is governed by

$$\Delta L = L\alpha_{th}\Delta T. \quad (2)$$

A hypothetical 7°C temperature change causes a 140 mm long aluminum fixture to expand by ~15 μm more than the glass foil inside of it. This difference distorts the foil if the holder forbids slip at the contact points (See Figure 3).

To estimate the reduction in foil warp from this expansion, the Figure 3 circle geometry can show that

$$\frac{2s}{c} = \frac{\theta}{\sin \frac{\theta}{2}} \quad (3)$$

Since $s=R\theta$, we can find R from the known s and c . Also from geometry,

$$h = R - R \cos \frac{\theta}{2} \quad (4)$$

Using $s=140$ mm and $c=139.985$ mm yields $h=888$ μm. This is much larger than the 0.5 μm tolerance. Thus, another functional requirement of the fixture design is that sliding between the foil and fixture must be permitted.

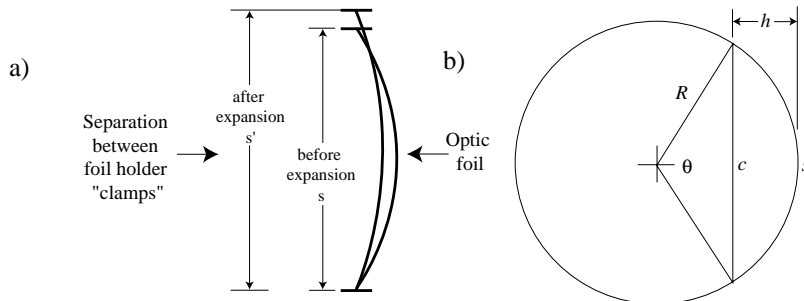


Figure 3. (a) Due to thermal expansion differences, the foil holder can reduce the foil warp if the boundary conditions do not allow slip. (b) The circle geometry is used to calculate this reduction.

1.6 Friction

Friction between foil and fixture can cause intolerable distortion. Consider an assembly scenario where a foil is slid into position by finger-like microstructure combs in accordance with other assembly research [3] (See Figure 4a). Comb teeth provide the actuation force, and friction arises from contact between the optic foil and comb base. Modeling as in Figure 4b, the friction force, $F_{friction}$ is

$$F_{friction} = \mu mg \quad (5)$$

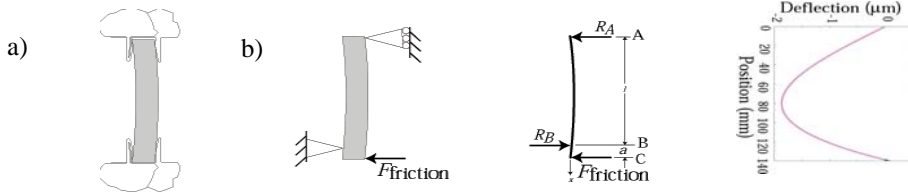


Figure 4. Forces from comb actuation and friction at the bottom of the foil can lead to distortion.

where μ , the coefficient of static friction, has been measured to be 0.39 [2]. The glass foil mass, m , is 14.1 g. The comb and foil dimensions are such that $a=1.09$ mm and $l=138.91$ mm. The maximum beam deflection is then

$$\delta_{\max} = \frac{F_{\text{friction}} a^2 (l+a)}{3EI} = 1.9 \mu\text{m} \quad (6)$$

An FEA simulation with the ball-socket triad gives $2.76 \mu\text{m}$, which compares well to the analytical result, indicating that friction can cause deformation beyond tolerances. A fixture design should therefore reduce or eliminate this friction. From these requirements, concept generation progressed to the design and fabrication of the foil fixture.

2. Experiment

The design of an optic foil holder with minimum friction forces is investigated. This holder utilizes two sets of air bearings, top and bottom, to kinematically constrain the foil's six degrees of freedom as shown in Figure 5.

2.1 Description

The top set consists of three pairs of circular, inherently-compensated, opposing air bearings to constrain translation along the x -axis and rotation about the y - and z -axes. Small air gaps between the bearing and the optic surface validates the use of viscous properties of air in describing the pressure within the bearing region. The viscous layer results in thrust due to the pressure distribution within this region as described by

$$p = p_1 \left[1 - \left\{ 1 - (p_{\text{atm}}/p_1)^2 \right\} \ln(r/r_1) / \ln(r_2/r_1) \right]^{1/2} \quad [4] \quad (7)$$

where p_{atm} is atmospheric pressure, p_1 is supply pressure, r_1 is inner radius, r_2 is outer radius, and r is distance from the center of the bearing as shown in Figure 6a. The load capacity of air bearings is proportional to the bearing area. This setup utilizes tubes with outer diameter of $635 \mu\text{m}$ to avoid gap variation associated with surface warp of the optics and thus reduce air bearing instability. Since the foils are held vertically, the load on the bearings is very small and the use of small diameter tubes is justified in the viscous region.

The bottom set consists of two inherently compensated, multiple inlet, circular bearings that constrain translation and rotation along the z - and x -axes respectively. These bearings have almost zero stiffness along the lateral direction, which allows them to adjust with lateral motion caused by thermal expansion mismatch and foil placement friction. The current design utilizes four feedholes with dimensions shown in Figure 6b. The load on these bearings is small, so vacuum preloading is used to increase stiffness.

2.2 Procedure

The top set is divided into reference and spring bearings. The reference bearings are stationary and initially use vacuum to hold the foils vertically. The spring bearings face the reference ones and are pneumatically actuated in the x -direction to facilitate insertion of optics. As the spring bearing approaches the optic, thrust forces increase. A

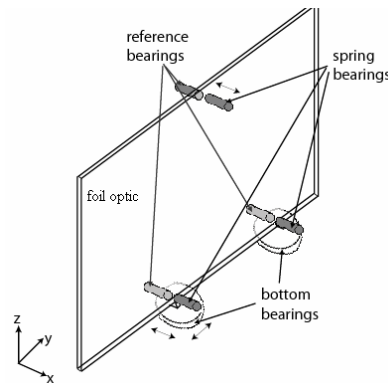


Figure 5. Two sets of air bearings, top and bottom, are used to kinematically constrain foil optics. The top set is divided into reference and spring bearings, which are exaggerated in size for clarity.

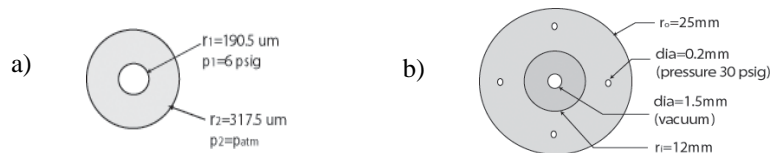


Figure 6. Geometry and dimensions of (a) top bearings and (b) bottom bearings.

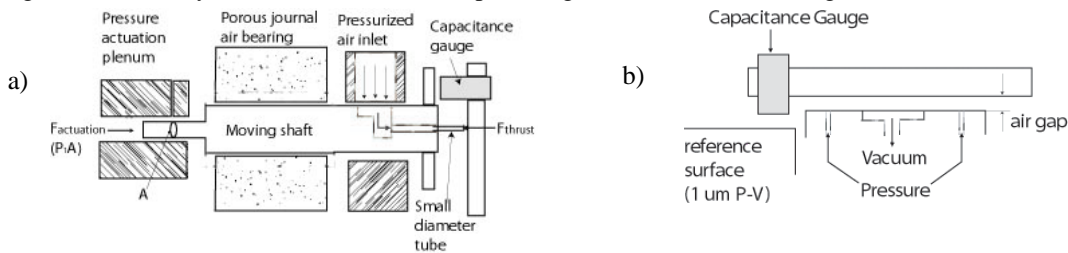


Figure 7. (a) Top bearing force versus gap calibration and (b) bottom bearing gap and stiffness vs vacuum calibration.

calibration curve is constructed for such bearings. A capacitance gauge is used to measure the gap between the air bearing and a conductive surface, and the force of actuation is equated to the thrust force in the absence of frictional forces, which are minimized by using a journal air bearing to carry the shaft of the top spring bearing as shown in Figure 7a. Contact between bearing and conducting surface is indicated by an electrical short circuit.

The actuating pressure is gradually decreased while the air gap is measured. Since the tube outer diameter is small, certain aspects must be altered to enhance the proper development of radial boundary layers that form the basis of the viscous flow between the two surfaces, such as the decrease in supply pressure and increase in tube inner diameter, to reduce the entrance effects of separation caused by the turning of the jet at the bearing exit. After proper positioning of the spring bearings, the reference bearings pneumatically center the foils.

The bottom bearing is supplied with air at 30 psig. Different vacuum pressures are used to study the stiffness of this configuration. A load of 55 g is applied to measure the decrease in air gap and calculate the stiffness. The gap is measured with a capacitance gauge as shown in Figure 7b.

2.3 Results

To ensure proper bearing performance, the flow of air must be within the viscous region, which can only be achieved at very small air gaps. Figure 8a shows that a gap of around 8 μm for the top bearing is sustained at pressures around 0.18 psig acting on a 2.54 mm diameter shaft. This calibrated curve depends on the spring bearing assembly orientation—pitch errors introduce the shaft weight, and therefore require a new calibration curve.

Figure 8b shows the effect of vacuum on the bottom bearing stiffness, which rises rapidly at lower vacuum levels and stabilizes at around 20 in Hg, providing a good operating region. The bearing has demonstrated some lateral instability due to the inherent property of negligible lateral stiffness of thrust bearings.

3. Conclusions

The behavior of thin optics under loads such as gravity, thermal expansion, and friction has been presented as modeled analytically and using FEA. From these studies, the requirements for the design of a foil holder have been derived, and the essential element in this foil holder, the constraint bearings, have been design and evaluated.

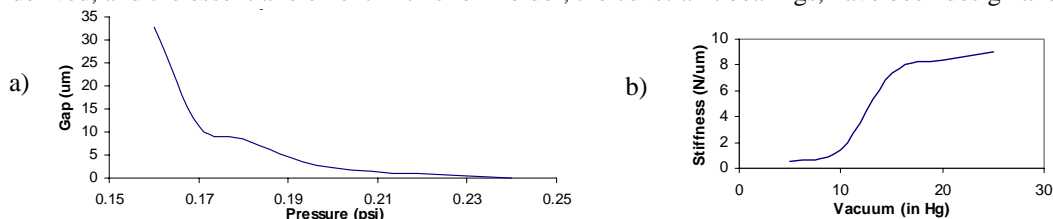


Figure 8. Plot of (a) air gap versus actuating pressure for top bearings and (b) stiffness versus vacuum for bottom bearings.

References

- [1] C.R. Forest et al., "Metrology of thin transparent optics using Shack-Hartmann wavefront sensing," Submitted to Optical Engineering (2003).
- [2] O. Mongrard. High accuracy foil optics for x-ray astronomy. Master's Thesis, MIT, September 2001.
- [3] C.R. Forest et al., "Precision assembly and metrology of x-ray foil optics," Proc. of 17th Annual ASPE (2002).
- [4] W.A. Gross, "Gas Film Lubrication," John Wiley and Sons, Inc (1962).
- [5] M. Fourka and M. Bonis, "Comparison between externally pressurized gas thrust bearings with different orifice and porous feeding systems," Wear, 210, 311-317 (1997).